



**Aqueous ROPISA of aminoacid N-carboxyanhydrides:  
polypeptide block secondary structure controls nanoparticle  
shape anisotropy**

Journal:	<i>Polymer Chemistry</i>
Manuscript ID	PY-ART-07-2021-000995.R1
Article Type:	Paper
Date Submitted by the Author:	14-Sep-2021
Complete List of Authors:	Grazon, Chloé; Université de Bordeaux, ISM Salas-Ambrosio, Pedro; University of Bordeaux, ENSCBP, LCPO Antoine, Ségolène; University of Bordeaux, ENSCBP, LCPO Ibarboure, Emmanuel; University of Bordeaux, ENSCBP, LCPO Sandre, Olivier; Université de Bordeaux, ENSCBP, LCPO Clulow, Andrew; Monash Institute of Pharmaceutical Sciences, Drug Delivery, Disposition and Dynamics Boyd, Ben; Monash University, Monash Institute of Pharmaceutical Sciences Grinstaff, Mark; Boston University, Dept of Biomedical Engineering + Chemistry Lecommandoux, Sébastien; University of Bordeaux, ENSCBP, LCPO Bonduelle, Colin; University of Bordeaux, ENSCBP, LCPO

# Aqueous ROPISA of $\alpha$ -aminoacid *N*- carboxyanhydrides: polypeptide block secondary structure controls nanoparticle shape anisotropy

*Chloé Grazon,<sup>‡a,b,c</sup> Pedro Salas-Ambrosio,<sup>‡a</sup> Segolene Antoine,<sup>a</sup> Emmanuel Ibarboure,<sup>a</sup>*

*Olivier Sandre,<sup>a</sup> Andrew J. Clulow,<sup>d,e</sup> Ben J. Boyd,<sup>d,f</sup> Mark W. Grinstaff,<sup>b</sup> Sébastien*

*Lecommandoux,<sup>\*a</sup> Colin Bonduelle.<sup>\*a</sup>*

<sup>a</sup> Univ. Bordeaux, CNRS, Bordeaux INP, LCPO, UMR 5629, F-33600, Pessac, France.

<sup>b</sup> Departments of Chemistry and Biomedical Engineering, Boston University, Boston, MA (USA)

<sup>c</sup> Univ. Bordeaux, Institut des Sciences Moléculaires (CNRS UMR 5255), 33405 Talence, France.

<sup>d</sup> Drug Delivery, Disposition and Dynamics, Monash Institute of Pharmaceutical Sciences, 381 Royal Parade, Parkville, VIC 3052, Australia

<sup>e</sup> Australian Synchrotron, ANSTO, 800 Blackburn Road, Clayton, VIC 3168, Australia.

<sup>f</sup> ARC Centre of Excellence in Convergent Bionano Science and Technology, Monash Institute of Pharmaceutical Sciences, 381 Royal Parade, Parkville, VIC 3052, Australia

<sup>‡</sup> co-first authors

KEYWORDS: ROPISA,  $\alpha$ -aminoacid *N*-carboxyanhydride, Polypeptide, Amphiphilic polymers, Self-assembly, Secondary structure, Small-Angle X-ray Scattering, Wide-Angle X-ray Scattering

ABSTRACT. Polymerization-induced self-assembly (PISA) is an efficient one-step process to obtain nanomaterials. In this work, aqueous ring-opening polymerization induced self-assembly (ROPISA) of  $\alpha$ -aminoacid *N*-carboxyanhydride (NCA) affords controllable well-defined nanoassemblies. ROPISA with the PEG<sub>5kDa</sub>-NH<sub>2</sub> macroinitiator and either the benzyl-*L*-glutamate NCA (BLGNCA) or *L*-leucine NCA (LeuNCA) monomer yields amphiphilic block copolymers, with different polypeptide molar masses, which spontaneously form nanostructures. In contrast to the previous PISA process where the hydrophobic to hydrophilic ratio was the main parameter defining nanomaterial morphology, the secondary structure of the polypeptides is the main driving force to stabilize the anisotropic rod-like nanostructures with this ROPISA process.

**1. Introduction.** Self-assembly is a fundamental process in which simple chemical components, called building blocks (molecules, colloids, polymers...) spontaneously organize themselves into objects of well-defined morphology in a process that is driven by key physico-chemical interactions.<sup>1</sup> In polymer science, appropriate use of both complementary and antagonistic interactions, together with specific entropic constraints related to macromolecular systems, will efficiently induce self-assembly over many length scales.<sup>2,3</sup> Self-assembly is generally a two-step methodology: first is the design of specific building blocks encoding chemical information (amphiphilic copolymers, etc.) and the second is their spontaneous organization through solvent-induced effects and/or the stepwise formation of noncovalent weak chemical bonds.<sup>4-8</sup> Synthetic polypeptides are among the most versatile building blocks to conceive nanomaterials in aqueous solution, a key solvent system required for biomedical applications: they offer a unique way to guide the formation of self-assembled systems through biomimetic structuring.<sup>9-11</sup> Moreover, polypeptides combine advantageous features of synthetic polymers (solubility, process, rubber elasticity, etc.) with those of natural proteins (secondary structure, functionality, biocompatibility, etc.).<sup>12-15</sup> The ability to precisely design polypeptides fitting a particular function is one of their greatest strengths, and the combination of ring-opening polymerization and self-assembly currently paves the way towards unprecedented possibilities to scale-up the synthesis of functional nanomaterials.<sup>16-19</sup>

In this context, polymerization-induced self-assembly (PISA) is a recent method for producing amphiphilic block copolymers and nano-objects.<sup>20,21</sup> PISA is the *in situ* growth of a living amphiphilic polymer chain during its self-assembly into nanostructures.<sup>22</sup> This method, thus, offers many advantages compared to other conventional polymerization routes for facile preparation of nanoparticles with high solid contents ( $\tau$ ), enabling massive production in one-step. To date, PISA

is accomplished predominantly using controlled radical polymerization processes,<sup>23–25</sup> such as RAFT polymerization in dispersion<sup>26,27</sup> or emulsion.<sup>28,29</sup> PISA is attracting interest in a broad range of fields from polymer chemistry, rheology, optics, to biology and, as a direct consequence, PISA offers a unique route to materials for broad ranges of applications.<sup>30,31</sup> Whereas PISA is an outstanding process for nanomaterial preparation, examples in the literature involving its specific application to ring-opening polymerization (ROP) are scarce. Yet, ROP is one the best synthetic processes to introduce favourable features including the biodegradability of polymers.<sup>32–36</sup> However, ROP is a more laborious process to implement when compared with radical polymerization, especially in aqueous media, which limits its development. Recently, aqueous PISA was successfully performed with Ring-Opening Metathesis Polymerization (ROMPISA) but the resulting nanoparticles were not biodegradable.<sup>37</sup> From our laboratory, we reported Ring-Opening Polymerization-Induced Self-Assembly (ROPISA) in aqueous buffer using  $\gamma$ -benzyl-*L*-glutamate *N*-carboxyanhydrides (BLG-NCA) in the presence of  $\alpha$ -amino-poly(ethylene oxide) initiators.<sup>33</sup> This new NCA monomer polymerization process in aqueous conditions is exciting as we successfully controlled unwanted water-induced NCA ring-opening by the formation of protective micelles. Herein, we report a comprehensive study of this aqueous ROPISA process by preparing a small library of polypeptides from two NCA monomers, derived from benzyl-*L*-glutamate (BLG-NCA) and *L*-Leucine (Leu-NCA), and a hydrophilic macromer initiator with varying the degrees of polymerization (as predetermined by the  $[M]/[I]$  ratio of monomer to initiator; see scheme 1). Our results show that the secondary peptide structure, e.g. BLG-NCA giving rise to  $\alpha$ -helix-structured polypeptides while Leu-NCA to  $\beta$ -sheet-structured polypeptides, controls the nanomaterial morphologies and their anisotropy.

## 2. Experimental

*a) Materials and methods*

All chemicals were purchased from Sigma-Aldrich and used as received unless otherwise noted. Solvents *N,N*-dimethylformamide (DMF) and hexafluoropropan-2-ol (HFIP) were bought from Sigma.  $\gamma$ -Benzyl-*L*-glutamate *N*-carboxyanhydride (BLG-NCA) and *L*-leucine *N*-carboxyanhydride (Leu-NCA) were supplied from PMC Isochem (Vert-le-Petit, France). PEG<sub>5k</sub>-NH<sub>2</sub> (Mp = 5516 g·mol<sup>-1</sup>,  $D = 1.02$ ) was bought from RAPP Polymer Gmbh (Tübingen, Germany). Ultra-pure water was obtained from a Milli Q system (Purelab Prima, ELGA, France) with a resistivity of 18.2 M $\Omega$ . <sup>1</sup>H NMR spectra were recorded at room temperature with a Bruker Avance 400 (400 MHz). CDCl<sub>3</sub> with TFA was used as solvent and signals were referred to the signal of residual protonated solvent signals. **Fourier Transformed Infrared Spectroscopy – Attenuated Total Reflection (FTIR-ATR)**. FTIR spectra were collected on a Bruker Vertex 70 spectrometer equipped with a diamond ATR tool in the spectral region of 900-2000 cm<sup>-1</sup> from 32 scans with a resolution of 4 cm<sup>-1</sup>. A background was recorded before loading the samples onto the ATR crystal for measurements. FTIR of copolymers dialyzed and lyophilized powders were measured using air as background. **Size Exclusion Chromatography (SEC)**. Polymer molar masses were determined by SEC using dimethylformamide (DMF + LiBr 1 g·L<sup>-1</sup>) or hexafluoro-2-propanol (HFIP+ 0,05% KTFA) as eluent. Measurements in DMF were performed on an Ultimate 3000 system from ThermoFischer Scientific (Ilkirch, France) equipped with a diode array detector (DAD). The system also includes a multi-angle light scattering detector (MALS) and differential refractive index detector dRI from Wyatt technology (Santa Barbara CA, USA). Polymers were separated on three Shodex Asahipack gel columns [GF 310 (7.5 × 300 mm), GF510 (7.5×300), exclusion limits from 500-300 000 Da] at a flowrate of 0.5 mL/min. Columns temperature was held at 50°C. Easivial™ kit of Polystyrene from Agilent (Santa Clara CA, USA)

was used as calibration standard ( $M_n$  from 162 to 364 000 Da). Measurements in HFIP were performed on similar equipment as DMF analyses with the same components: DAD, MALS dRI. Polymers were separated on a PL HFIP gel columns ( $300 \times 7.5$  mm), exclusion limits from 100 Da to 150 000 Da at a flowrate of  $0.8 \text{ mL} \cdot \text{min}^{-1}$ . Columns temperature was held at  $40^\circ\text{C}$ . Easivial™ kit of PMMA from Agilent (Santa Clara CA, USA) was used as calibration standard ( $M_n$  from 1800 to 256 000 Da). Refractive index increment ( $dn/dc$ ) of the copolymer PEG-*b*-PBLG in DMF + LiBr  $1 \text{ g} \cdot \text{L}^{-1}$  were estimated according to our previous work.<sup>33</sup> **Atomic Force Microscopy (AFM)** measurements were performed at room temperature in a dry state using a Multimode 8™ microscope (Veeco Instruments Inc., Bruker, Santa Barbara CA, USA). Both topographic and phase images of needle-like nanoparticles were obtained in Tapping Mode™ using rectangular silicon cantilever (AC 160-TS, Atomic Force Microscopy probes Asylum, Wiesbaden, Germany) with a spring constant of  $26 \text{ N} \cdot \text{m}^{-1}$ , a resonance frequency lying in the 270-320 kHz range and a radius of curvature of less than 10 nm. Samples were prepared by solvent casting at ambient temperature from a stock solution ( $70 \text{ mg} \cdot \text{mL}^{-1}$ ). A drop ( $5 \mu\text{L}$ ) of suspension was deposited onto freshly cleaved mica, and after 10 minutes the excess of solution was removed with blotting paper. Subsequently, the substrate was dried under nitrogen flow for several minutes. Measurements of particle lengths and widths were made using the Particle Analysis tool provided with the AFM software (Nanoscope Analysis V1.20 from Bruker). **CryoTEM** Cryo-Transmission Electron Microscopy (cryo-TEM) micrographs were obtained as follows: a drop of suspension was deposited on a “Quantifoil”® (Quantifoil Micro Tools GmbH, Germany) carbon membrane. The excess of liquid on the membrane was blotted with filter paper and the membrane was quenched-frozen quickly in liquid ethane to form a thin vitreous ice film including NPs in the holes of the grid. Once placed in a Gatan 626 cryo-holder cooled with liquid nitrogen, the samples were

transferred into the microscope and observed at low temperature ( $-180\text{ }^{\circ}\text{C}$ ). Cryo-TEM images were recorded on an Ultrascan 2kpixel CCD camera (Gatan, USA), using a LaB6 JEOL 2100 (JEOL, Japan) cryo microscope operating at 200 kV with a JEOL low dose system (Minimum Dose System, MDS) to protect the thin ice film from any irradiation before imaging and reduce the irradiation during the image capture. **Dynamic Light Scattering (DLS)** The hydrodynamic diameter ( $D_h$ ) and the polydispersity index (PDI) of the nanoparticles were determined by DLS with a Zetasizer Nano ZS from Malvern Instruments (Malvern, UK) operating with a He-Ne laser source (wavelength 633 nm, scattering angle  $90^{\circ}$ ). The correlation functions were analysed using the cumulant method. The dispersions were analysed at 0.1 wt % in water after filtration on a 1  $\mu\text{m}$  glass filter. **Transmission Electron Microscopy (TEM)** The images were recorded on a Hitachi H7650 microscope working at 80 kV. Samples were prepared by spraying a  $1\text{ g}\cdot\text{L}^{-1}$  solution of the block copolymer onto a copper grid (200 mesh coated with carbon) using a homemade spray tool and negatively stained with 1% uranyl acetate. **Small and wide angle X-ray scattering (SAXS/WAXS)** profiles were acquired on the SAXS/WAXS beam line at the Australian Synchrotron (part of ANSTO) in Clayton, Australia.<sup>38</sup> All measurements were performed at the ambient temperature of the SAXS/WAXS experimental hutch, which is typically around  $27\text{ }^{\circ}\text{C}$ . The samples were drawn one at a time into a quartz capillary (1.5 mm diameter) held stationary in the X-ray beam (photon energy = 13.0 keV, wavelength  $\lambda = 0.954\text{ \AA}$ ) and scattering measurements were performed. After each sample, the capillary was washed with ethanol ( $\times 3$ ), water ( $\times 1$ ), the solvent mixture for the samples ( $\times 2$ ) and the next sample ( $\times 1$ ) before the next sample was loaded and measured. Scattering at low  $q$  values was recorded at a sample-detector distance of 7384 mm and scattering at higher- $q$  values was recorded with a sample-detector distance of 795 mm. 2D scattering patterns were recorded using a Pilatus 2Mpixel detector



and radially integrated into scattering functions  $I(q)$  versus  $q$  using the in-house developed software package ScatterBrain. The scattering functions were plotted on an absolute scale with units of  $\text{cm}^{-1}$  using the scattering from water in the sampling capillary as a standard. The low- and high- $q$  data were stitched together using the IRENA data analysis suite (Version 2.61)<sup>38</sup> in the IgorPro 7 environment to give scattering profiles with a continuous  $q$ -range from 0.002 – 1.940  $\text{\AA}^{-1}$ . The scattering profiles were analysed using the SASView fitting software (Version 4.2.2)<sup>39</sup> using the theoretical form factor of polydisperse cylinders.<sup>39</sup>

### *b) Synthesis*

**Typical synthesis procedure of poly(ethylene glycol)-*b*-poly( $\gamma$ -benzyl-*L*-glutamate) PEG-*b*-PBLG<sub>22</sub>.** In a glove box, the NCA monomer of  $\gamma$ -benzyl-*L*-glutamate (300 mg, 1.14 mmol) was weighed in a Schlenk tube containing a magnetic stirring bar. The Schlenk was removed from the glove box and cooled on ice. Then 8 mL of an ice-cooled solution of  $\text{NaHCO}_3$  0.05 M containing the initiator  $\text{PEG}_{5k}\text{-NH}_2$  (300 mg, 0.06 mmol,  $[\text{M}]/[\text{I}] = 19$ ) was added to the BLG-NCA powder under a strong agitation (solid content,  $\tau = 7\%$ ). The reaction was left to stir 1) first in an ice-cold water bath; 2) then at room temperature overnight. The opalescent dispersion obtained was then transferred to a 3.5 kDa dialysis membrane and dialysed against deionised water for 2 days. An aliquot was kept for hydrodynamic size analysis by DLS and further observation (AFM, TEM), and the remaining dispersion was lyophilized. A white powder was obtained with a yield of 87%. Molar mass ( $M_n$ ) was first determined by  $^1\text{H}$  NMR (see figure S1) using the equation 1:

$$M_n = DP_{\text{BLG}} \times (219 \text{ g/mol}) + DP_{\text{PEG}} \times (44 \text{ g/mol}) \quad \text{Eq. 1}$$

$$dP = \frac{1}{n} \sum_{i=1}^n iH \quad \text{Eq. 2}$$

Where degree of polymerization -  $DP$  values in equation 2 are the averaged degree of polymerization, calculated by integration of the polymer backbone protons  $iH$  for both PBLG and PEG blocks. Therefore, a PBLG degree of polymerization was calculated  $DP_{\text{BLG}}=22$  and a molar mass of the copolymer  $M_n=10690 \text{ g}\cdot\text{mol}^{-1}$ . The number-average molecular weight measured by SEC was  $M_n=11940 \text{ g}\cdot\text{mol}^{-1}$  (calibration with polystyrene standards) or  $9360 \text{ g}\cdot\text{mol}^{-1}$  (absolute measurement with MALS detection), and the calculated molar mass dispersity was  $D=1.10$  (see figure S2).  $^1\text{H}$  NMR (400 MHz,  $\text{CDCl}_3$  15% TFA,  $\delta$ , ppm): 7.85 (b, 1H, NH), 7.28 (b, 5H, Ar), 5.08 (q, 2H,  $\text{CH}_2$ ), 4.60 (b, 1H, CH), 3.70 (s, 4H, O- $\text{CH}_2\text{CH}_2$ ), 3.52 (s, 3H,  $\text{CH}_3$ ), 2.44 (b, 2H,  $\text{CH}_2$ ), 2.11-1.91 (b, 2H,  $\text{CH}_2$ ).

**Typical synthesis procedure of poly(ethylene glycol)-*b*-poly( $\gamma$ -benzyl-*L*-glutamate) PEG-*b*-PBLG<sub>11</sub>.** This copolymer was prepared by the same method as described above for copolymer PEG-*b*-PBLG<sub>22</sub> except that the amount of PEG<sub>5k</sub>-NH<sub>2</sub> was different (75 mg, 0.015 mmol,  $[M]/[I] = 5$ ). Yield: 63%.  $^1\text{H}$  NMR (400 MHz,  $\text{CDCl}_3$  15% TFA,  $\delta$ , ppm): 7.85 (b, 1H, NH), 7.28 (b, 5H, Ar), 5.08 (q, 2H,  $\text{CH}_2$ ), 4.60 (b, 1H, CH), 3.70 (s, 4H, O- $\text{CH}_2\text{CH}_2$ ), 3.52 (s, 3H,  $\text{CH}_3$ ), 2.44 (b, 2H,  $\text{CH}_2$ ), 2.11-1.91 (b, 2H,  $\text{CH}_2$ ). According to method described for PEG-*b*-PBLG<sub>22</sub>, a PBLG degree of polymerization was calculated from  $^1\text{H}$  NMR ( $DP_{\text{BLG}}=11$ ) and SEC then provided a number-average molecular weight  $M_n$  of  $4990 \text{ g}\cdot\text{mol}^{-1}$  (MALS) and  $D=1.17$  (see figure S2).

**Typical synthesis procedure of poly(ethylene glycol)-*b*-poly( $\gamma$ -benzyl-*L*-glutamate) PEG-*b*-PBLG<sub>15</sub>.** This copolymer was prepared by the same method as described above for copolymer

**PEG-*b*-PBLG<sub>22</sub>** except that the amount of PEG<sub>5k</sub>-NH<sub>2</sub> was different (150 mg, 0.03 mmol, [M]/[I] = 10). Yield: 70%. <sup>1</sup>H NMR (400 MHz, CDCl<sub>3</sub> 15% TFA, δ, ppm): 7.85 (b, 1H, NH), 7.28 (b, 5H, Ar), 5.08 (q, 2H, CH<sub>2</sub>), 4.60 (b, 1H, CH), 3.70 (s, 4H, O-CH<sub>2</sub>CH<sub>2</sub>), 3.52 (s, 3H, CH<sub>3</sub>), 2.44 (b, 2H, CH<sub>2</sub>), 2.11-1.91 (b, 2H, CH<sub>2</sub>). According to method described for **PEG-*b*-PBLG<sub>22</sub>**, a PBLG degree of polymerization was calculated from <sup>1</sup>H NMR ( $DP_{\text{BLG}}=15$ ) and SEC then provided a number-average molecular weight  $M_n$  of 7700 g·mol<sup>-1</sup> (MALS) and  $D=1.12$  (see figure S2).

**Typical synthesis procedure of poly(ethylene glycol)-*b*-poly( $\gamma$ -benzyl-*L*-glutamate) PEG-*b*-PBLG<sub>43</sub>.** This copolymer was prepared by the same method as described above for copolymer **PEG-*b*-PBLG<sub>22</sub>** except that the amount of PEG<sub>5k</sub>-NH<sub>2</sub> was different (600 mg, 0.12 mmol, [M]/[I] = 38). Yield: 42%. <sup>1</sup>H NMR (400 MHz, CDCl<sub>3</sub> 15% TFA, δ, ppm): 7.85 (b, 1H, NH), 7.28 (b, 5H, Ar), 5.08 (q, 2H, CH<sub>2</sub>), 4.60 (b, 1H, CH), 3.70 (s, 4H, O-CH<sub>2</sub>CH<sub>2</sub>), 3.52 (s, 3H, CH<sub>3</sub>), 2.44 (b, 2H, CH<sub>2</sub>), 2.11-1.91 (b, 2H, CH<sub>2</sub>). According to method described for **PEG-*b*-PBLG<sub>22</sub>**, a PBLG degree of polymerization was calculated from <sup>1</sup>H NMR ( $DP_{\text{BLG}}=43$ ) and SEC then provided a number-average molecular weight  $M_n$  of 12570 g·mol<sup>-1</sup> (MALS) and a  $D=1.15$  (see figure S2).

**Typical synthesis procedure of poly(ethylene glycol)-*b*-poly( $\gamma$ -benzyl-*DL*-glutamate) PEG-*b*-PBDLG.** This copolymer was prepared by the same method as described above for copolymer **PEG-*b*-PBLG<sub>22</sub>** except that a racemic mixture of  $\gamma$ -benzyl glutamate-derived NCA monomer was used (PEG<sub>5k</sub>-NH<sub>2</sub>, 300 mg, 0.06 mmol, [M]/[I] = 19). Yield: 71%. <sup>1</sup>H NMR (400 MHz, CDCl<sub>3</sub> 15% TFA, δ, ppm): 7.85 (b, 1H, NH), 7.28 (b, 5H, Ar), 5.08 (q, 2H, CH<sub>2</sub>), 4.60 (b, 1H, CH), 3.70 (s, 4H, O-CH<sub>2</sub>CH<sub>2</sub>), 3.52 (s, 3H, CH<sub>3</sub>), 2.44 (b, 2H, CH<sub>2</sub>), 2.11-1.91 (b, 2H, CH<sub>2</sub>). According to method described for **PEG-*b*-PBLG<sub>22</sub>**, a degree of polymerization was calculated from <sup>1</sup>H NMR ( $DP_{\text{BLG}}=19$ ) and SEC then provided a number-average molecular weight  $M_n$  of 7700 g·mol<sup>-1</sup> (PMAM calibration curve) and  $D=1.15$  (see figure S15).

**Typical synthesis procedure of poly(ethylene glycol)-*b*-poly(*L*-Leucine) PEG-*b*-PLLeu<sub>26</sub>.**

In a glove box, the NCA monomer of *L*-Leucine (Leu-NCA, 300 mg, 1.9 mmol) is weighed in a Schlenk tube containing a magnetic stirring bar. The Schlenk was removed from the glove box and cooled on ice. Then 8 mL of an ice-cooled solution of NaHCO<sub>3</sub> 0.05M containing the initiator PEG5k-NH<sub>2</sub> (300 mg, 0.06 mmol, [M]/[I] = 32) was added to the NCA powder under a strong agitation (solid content,  $\tau = 7\%$ ). The reaction is left to stir 1) first in an ice-cold water bath; 2) then at room temperature overnight. The opalescent dispersion obtained was then transferred to a 3.5 kDa dialysis membrane and dialysed against deionised water for 2 days. An aliquot was kept for further microscopy imaging and dynamic light scattering and the remaining dispersion was lyophilized. A white powder was obtained with a yield of 77%. Molar mass ( $M_n$ ) was first determined by <sup>1</sup>H NMR (see figure S3) using:

$$M_n = DP_{\text{Leu}} \times (113 \text{ g/mol}) + DP_{\text{PEG}} \times (44 \text{ g/mol}) \quad \text{Eq. 3}$$

The  $DP$  values in equation 3 are calculated by integration of the polymer backbone protons  $iH$  for both PLeu and PEG blocks, resulting in a PLeu degree of polymerization  $DP_{\text{Leu}}=26$  and a molar mass of the copolymer calculated by NMR  $M_n=8673 \text{ g/mol}$ . SEC then provided a number-average molar mass  $M_n$  of  $9360 \text{ g mol}^{-1}$  (PMAM calibration curve) and a molar mass dispersity  $D=1.18$  (see figure S4). <sup>1</sup>H NMR (400 MHz, CDCl<sub>3</sub> 30% TFA,  $\delta$ , ppm): 7.73 (b, 1H, NH), 4.57 (b, 1H, CH), 3.80 (s, 4H, O-CH<sub>2</sub>CH<sub>2</sub>), 3.52 (s, 3H, CH<sub>3</sub>), 1.53 (b, 2H, CH<sub>2</sub>), 0.91-0.85 (b, 7H, -CH-(CH<sub>3</sub>)<sub>2</sub>).

**Typical synthesis procedure of poly(ethylene glycol)-*b*-poly(*L*-Leucine) PEG-*b*-PLLeu<sub>16</sub>.** This copolymer was prepared by the same method as described above for copolymer PEG-*b*-PLLeu<sub>26</sub>

except that the amount of PEG5k-NH<sub>2</sub> was different (150 mg, 0.03 mmol, [M]/[I] = 16). Yield: 75%. <sup>1</sup>H NMR (400 MHz, CDCl<sub>3</sub> 30% TFA, δ, ppm): 7.73 (b, 1H, NH), 4.57 (b, 1H, CH), 3.80 (s, 4H, O-CH<sub>2</sub>CH<sub>2</sub>), 3.52 (s, 3H, CH<sub>3</sub>), 1.53 (b, 2H, CH<sub>2</sub>), 0.91-0.85 (b, 7H, -CH-(CH<sub>3</sub>)<sub>2</sub>). According to method described for **PEG-*b*-PLLeu<sub>26</sub>**, a PLeu degree of polymerization was calculated from <sup>1</sup>H NMR ( $DP_{Leu}=16$ ) and SEC then provided a number-average molecular weight  $M_n$  of 11040 g·mol<sup>-1</sup> (PMAM calibration curve) and  $\bar{D}=1.20$  (see figure S4).

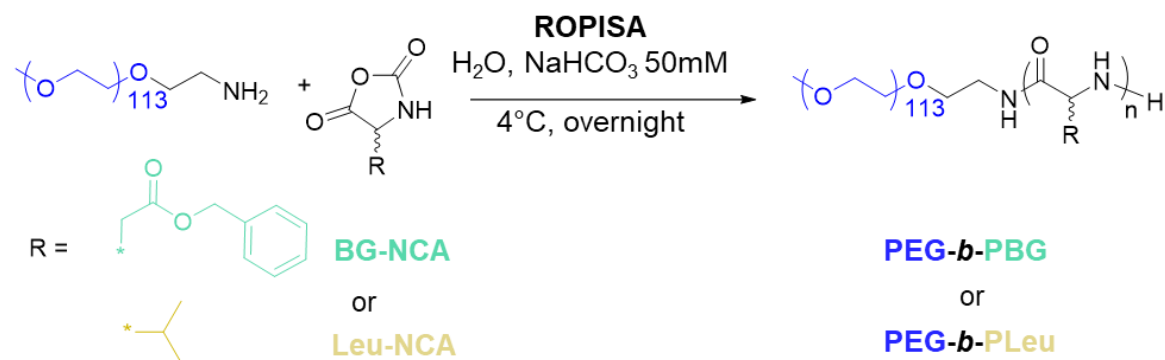
**Typical synthesis procedure of poly(ethylene glycol)-*b*-poly(*L*-Leucine) PEG-*b*-PLLeu<sub>46</sub>.** This copolymer was prepared by the same method as described above for copolymer **PEG-*b*-PLLeu<sub>26</sub>** except that the amount of PEG<sub>5k</sub>-NH<sub>2</sub> was different (450 mg, 0.09 mmol, [M]/[I] = 48). Yield: 29%. <sup>1</sup>H NMR (400 MHz, CDCl<sub>3</sub> 30% TFA, δ, ppm): 7.73 (b, 1H, NH), 4.57 (b, 1H, CH), 3.80 (s, 4H, O-CH<sub>2</sub>CH<sub>2</sub>), 3.52 (s, 3H, CH<sub>3</sub>), 1.53 (b, 2H, CH<sub>2</sub>), 0.91-0.85 (b, 7H, -CH-(CH<sub>3</sub>)<sub>2</sub>). According to method described for **PEG-*b*-PLLeu<sub>26</sub>**, a PLeu degree of polymerization was calculated from <sup>1</sup>H NMR ( $DP_{Leu}=46$ ) and SEC then provided a number-average molecular weight  $M_n$  of 13360 g·mol<sup>-1</sup> (PMAM calibration curve) and  $\bar{D}=1.17$  (see figure S4).

**Typical synthesis procedure of poly(ethylene glycol)-*b*-poly(*DL*-Leucine) PEG-*b*-PDL-Leu<sub>26</sub>.** This copolymer was prepared by the same method as described above for copolymer **PEG-*b*-PLLeu<sub>26</sub>** except that a racemic mixture of leucine-derived NCA monomer was used (PEG<sub>5k</sub>-NH<sub>2</sub>, 300 mg, 0.06 mmol, [M]/[I] = 32). Yield: 94%. <sup>1</sup>H NMR (400 MHz, CDCl<sub>3</sub> 30% TFA, δ, ppm): 7.73 (b, 1H, NH), 4.57 (b, 1H, CH), 3.80 (s, 4H, O-CH<sub>2</sub>CH<sub>2</sub>), 3.52 (s, 3H, CH<sub>3</sub>), 1.53 (b, 2H, CH<sub>2</sub>), 0.91-0.85 (b, 7H, -CH-(CH<sub>3</sub>)<sub>2</sub>). According to method described for **PEG-*b*-PLLeu<sub>26</sub>**, a PLeu degree of polymerization was calculated from <sup>1</sup>H NMR ( $DP_{Leu}=26$ ) and SEC then provided a number-average molecular weight  $M_n$  of 12500 g·mol<sup>-1</sup> (PMAM calibration curve) and  $\bar{D}=1.17$  (see figure S4).

### c) SAXS data analysis

The SAXS part of the X-ray scattering curves (*i.e.* over scattering vector  $q$  ranging from  $0.0025 \text{ \AA}^{-1}$  to  $0.25 \text{ \AA}^{-1}$ ) was analysed first. Whenever possible (*i.e.* when the curve showed plateauing at low  $q$  vectors), the radii of gyration of the different samples ( $R_G$ ) were determined by a linear fit of the curves in the Guinier representation (*i.e.* the logarithm of intensity *versus*  $q^2$  when  $q \rightarrow 0$ ), which slope is  $-R_G^2/3$ . Then SASView 4.2.2 program<sup>39</sup> was used to fit the curves (in the intermediate  $q$  range only when they exhibited an up-turn at low  $q$ ) with the theoretical cylinder form factors of length  $L$  and radius  $R$ ,<sup>40</sup> convoluted with Log-normal distributions of respective characteristic widths  $\sigma_L$  and  $\sigma_R$  (all other details being given in the supporting information part).

## 3. Results and discussion



**Scheme 1.** Ring-opening polymerization and *in situ* self-assembly (ROPISA) in water of BG-NCA or Leu-NCA monomers, initiated by a  $\alpha$ -amino-poly(ethylene oxide).

We first performed the aqueous ROPISA of the BLG-NCA monomer ( $[M]_0 = 0.14 \text{ M}$ ) in sodium bicarbonate aqueous buffer (pH 8.5, 50 mM) with  $\alpha$ -amino-poly(ethylene oxide) ( $\text{PEG}_{5k}\text{-NH}_2 = 5 \text{ kg}\cdot\text{mol}^{-1}$ ,  $M_n = 4.9 \text{ kDa}$ ,  $\text{Đ} = 1.08$ ) as the macromolecular initiator.<sup>33</sup> Starting at  $4^\circ\text{C}$  and upon extensive stirring, this procedure afforded an opalescent solution containing well-defined

diblock copolymers with narrow molar mass dispersity (**PEG-*b*-PBLG<sub>22</sub>**,  $M_n = 9360$  kDa,  $\mathcal{D} = 1.10$ , figure S1 and table 1) in good reaction yield (87%). Next, we synthesized a series of new diblock copolymers of varying PBLG block degree of polymerization (DP) from 11 to 43 using a similar procedure (table 1). Analyses of the copolymers by SEC in DMF and  $^1\text{H}$  NMR spectroscopy confirmed low molar mass dispersity ( $\mathcal{D}$ ) values between 1.12 and 1.17, and number-averaged molar mass  $M_n$  values relatively consistent with the change in the  $[\text{M}]/[\text{I}]$  ratio (see table 1 and fig. S1, S3-S6). Upon completion of ROPISA, we observed a bluish solution typical of multiple light scattering by concentrated nanoscale colloids (figure S12). It should be noted that for **PEG-*b*-PBLG<sub>43</sub>**, the reaction medium became highly viscous during ROPISA and resulted in the formation of a gel that was particularly difficult to collect for dialysis (figure S12). It is thus interesting to mention that other PISA reactions, already reported in literature, resulted in gels, whose origin was found to be the entanglement of "worm-like" morphologies.<sup>41</sup>

After a dialysis step to remove salts, we studied the suspensions of nanomaterials using different microscopic techniques. Firstly, atomic force microscopy (AFM) confirmed the presence of separated and individual nanorods with homogeneous lengths and diameters (**PEG-*b*-PBLG<sub>22</sub>**;  $65 \pm 8$  nm length with diameter of  $6 \pm 1$  nm) (figure S11). Next, we performed transmission electron microscopy (TEM) and cryo-TEM of the **PEG-*b*-PBLG** series and compared the images obtained with **PEG-*b*-PBLG<sub>22</sub>** in both the dry and wet states (figure 1). TEM images of **PEG-*b*-PBLG<sub>11</sub>**, with the shorter polypeptide block, showed small needle-like nanostructures, while the nanostructures of **PEG-*b*-PBLG<sub>15</sub>** exhibited slightly longer needle-like nanostructures. Increasing the **PBLG** length to 22 units (**PEG-*b*-PBLG<sub>22</sub>**) or 43 units (**PEG-*b*-PBLG<sub>43</sub>**) did not significantly modify the diameter of the nanorods. TEM microscopy revealed that the change in polypeptide

block DP resulted in modification of two key morphological parameters, length  $L$  and diameter  $d=2R$ , and thus the aspect ratio  $L/2R$ .

**Table 1.** Molar masses of diblock copolymers obtained by the ROPISA process at different  $[M]/[I]$  ratios using either BLG-NCA or Leu-NCA as the monomer.

Copolymer	Theory			<sup>1</sup> H NMR		SEC	
	$[M]/[I]$	$M_n$ g/mol	$\tau$ (%)	$DP$	$M_n$ g/mol	$M_n$ g/mol	$\bar{D}$
PEG- <i>b</i> -PBLG <sub>11</sub>	5	6040	4	11	8385	4990 <sup>a</sup>	1.17
PEG- <i>b</i> -PBLG <sub>15</sub>	10	7080	5	15	9297	7700 <sup>a</sup>	1.12
PEG- <i>b</i> -PBLG <sub>22</sub>	19	9160	7	22	10690	9360 <sup>a</sup>	1.10
PEG- <i>b</i> -PBLG <sub>43</sub>	38	13330	10	43	15011	12570 <sup>a</sup>	1.15
PEG- <i>b</i> -PBDLG	19	91160	7	19	9160	7700 <sup>a</sup>	1.15
PEG- <i>b</i> -PLL <sub>Leu16</sub>	16	6800	5	16	7769	11040 <sup>b</sup>	1.20
PEG- <i>b</i> -PLL <sub>Leu26</sub>	32	8600	7	26	8673	12510 <sup>b</sup>	1.18
PEG- <i>b</i> -PLL <sub>Leu46</sub>	48	10400	9	46	11191	13360 <sup>b</sup>	1.17
PEG- <i>b</i> -PDLL <sub>Leu</sub>	32	8600	7	26	8765	12500 <sup>b</sup>	1.17

<sup>a</sup> Determined in DMF + 1mg/mL LiBr with the static light scattering detector and calculated using the  $dn/dc$

estimated according to our previous work.<sup>33</sup> <sup>b</sup> Determined in HFIP and calculated using PMMA calibration curve.

Bloc copolymers are named by their degree of polymerizations determined by <sup>1</sup>H NMR.



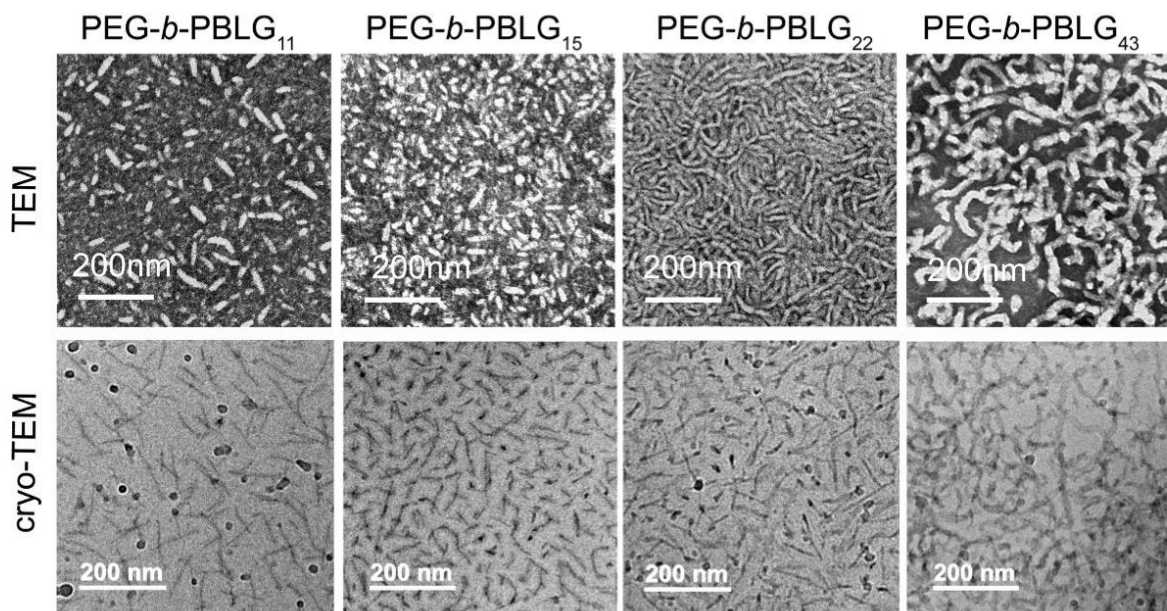


**Figure 1.** Electron microscopy images of the **PEG-*b*-PBLG** copolymer series obtained by ROPISA and dialyzed against ultra-pure water (top: TEM with negative staining using uranyl acetate, bottom: cryo-TEM).

To corroborate the microscopic observations, we next performed small-angle X-ray scattering (SAXS)<sup>42</sup> on the dispersions obtained upon ROPISA with all the **PEG-*b*-PBLG** copolymers (figure 2). The scattered intensity  $I$  as function of the wave vector  $q$  in a log-log representation tangents to a characteristic  $q^{-1}$  power law in the intermediate  $q$  range, hallmark of cylindrical structures, which was subsequently corroborated by more precise fitting of the data (figure S13). Using a theoretical model with a polydisperse cylinder form factor allowed us, in a second step, to extract putative values for the weight-average radius ( $R_w$ ) and the weight-average length ( $L_w$ ) of the nanometric rods (see table S1). According to TEM microscopy observations, the diameters of the nano objects did not appear significantly different at the different M/I ratio (7 to 10 nm). In electron microscopy, the small differences in diameters were ascribed to the solvated PEG layer which was negatively stained in TEM but which was neither observed in SAXS nor in cryo-TEM images (see figure 1).

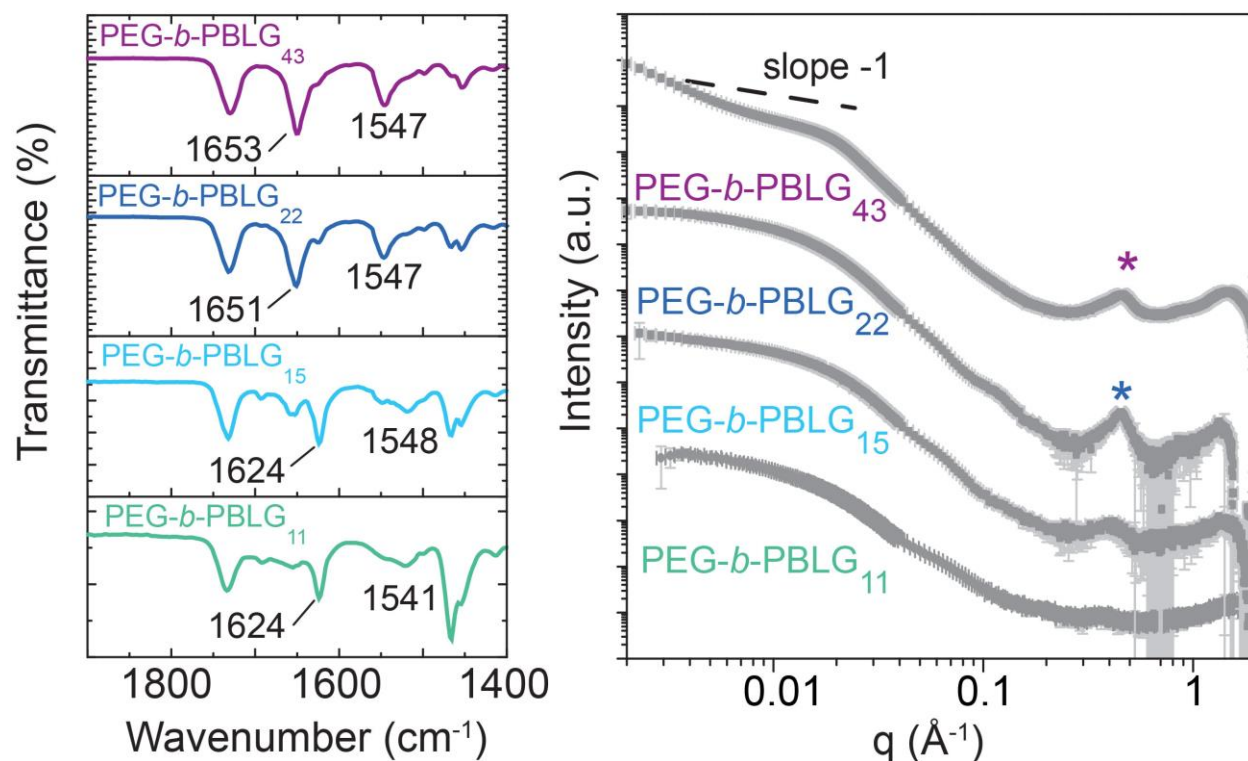


**Figure 2.** Copolymers **PEG-*b*-PBLG** analyzed by FTIR on lyophilized powders (left) or by small-angle X-ray scattering (SAXS) as nanoparticles in ultra-pure water (right). For sake of clarity, two successive curves are offset by 2 decades in logarithmic scale ( $\times 10^2$ ).

In the high  $q$  range (WAXS region), we observed a clear diffraction peak at  $q^*=0.457 \text{ \AA}^{-1}$  for **PEG-*b*-PBLG<sub>22</sub>** and **PEG-*b*-PBLG<sub>43</sub>** samples. This corresponded to a spacing of  $ca. 2\pi/q^*=13.7 \text{ \AA}$ , which we attributed to the repeating distance of a hexagonal array of PBLG  $\alpha$ -helices (a spacing of  $12.8 \text{ \AA}$  is expected)<sup>43–45</sup>. To corroborate the polypeptide conformation, we recorded the FTIR spectra of the lyophilized dried powders of all the PEG-*b*-PBLG copolymers (figure 2). In agreement with SAXS, copolymers **PEG-*b*-PBLG<sub>22</sub>** and **PEG-*b*-PBLG<sub>43</sub>** displayed amide I and II bands, typical of  $\alpha$ -helical conformation (amide I around  $1650 \text{ cm}^{-1}$  and amide II around  $1545 \text{ cm}^{-1}$ ). FTIR spectrum of the two shorter PBLG (copolymers **PEG-*b*-PBLG<sub>11</sub>** and **PEG-*b*-**

**PBLG<sub>15</sub>**) displayed amide bands typical of  $\beta$ -sheet conformations ( $1624\text{ cm}^{-1}$ ) which were attributed to the drying state as no clear Bragg-like peak in the scattering curves supported the occurrence of this secondary structure in aqueous suspension.<sup>11</sup> Finally, the aspect ratio between the length of the cylinder and its diameter was estimated and similar ratio values around 3 (table S1 in ESI) were found for copolymers **PEG-*b*-PBLG<sub>11-22</sub>**. Such precise value could not be estimated with the copolymer **PEG-*b*-PBLG<sub>43</sub>** forming a soft gel upon ROPISA with only an order of magnitude  $\sim 100$  ascribed to rod bundling (figure S12).

Synthetic polypeptide polymers adopt ordered secondary conformations such as  $\alpha$ -helices or  $\beta$ -sheets, a property that is rare in polymer science.<sup>11</sup> Tuning the secondary structures of polypeptides is a key strategy to modulate the physicochemical properties of self-assembly processes and to develop innovative materials.<sup>9,46-48</sup> To better understand the influence of this secondary structure in ROPISA, we performed the polymerization reactions with a second monomer, Leu-NCA, which forms a  $\beta$ -sheet-structured polypeptide. Maintaining the same solid content ( $\tau=7\%$ ), we first carried out the aqueous ROPISA of Leu-NCA ( $[M]_0 = 0.23\text{ M}$ ), under conditions similar to those used for **PEG-*b*-PBLG<sub>22</sub>**. We isolated a diblock copolymer with controlled molar mass dispersity (**PEG-*b*-PLLeu<sub>26</sub>**,  $M_n = 12510\text{ kDa}$ ,  $\mathcal{D} = 1.18$ , table 1) in good reaction yield (88%). After dialysis, we studied the nanomaterials by AFM and TEM. With both techniques, homogeneous nanoparticles with respect to size were obtained exhibiting elongated morphologies (figure 3 and S11). Comparatively, in TEM, nanoparticles of **PEG-*b*-PLLeu<sub>26</sub>** presented with a more anisotropic rod-like morphology than nanoparticles prepared from **PEG-*b*-PBLG<sub>22</sub>** (figure 3). AFM images confirmed the presence of separated and individual nanorods with homogeneous lengths and diameters ( $200 \pm 31\text{ nm}$  length with diameter of  $12 \pm 1\text{ nm}$ ) (figure S11). To confirm the conclusions drawn with the images obtained in a dried state, we also performed

cryo-TEM to study the morphology of the nanomaterials in their hydrated state (figure 3). These additional images confirm that our first ROPISA of Leu-NCA affords more elongated nanomaterials.

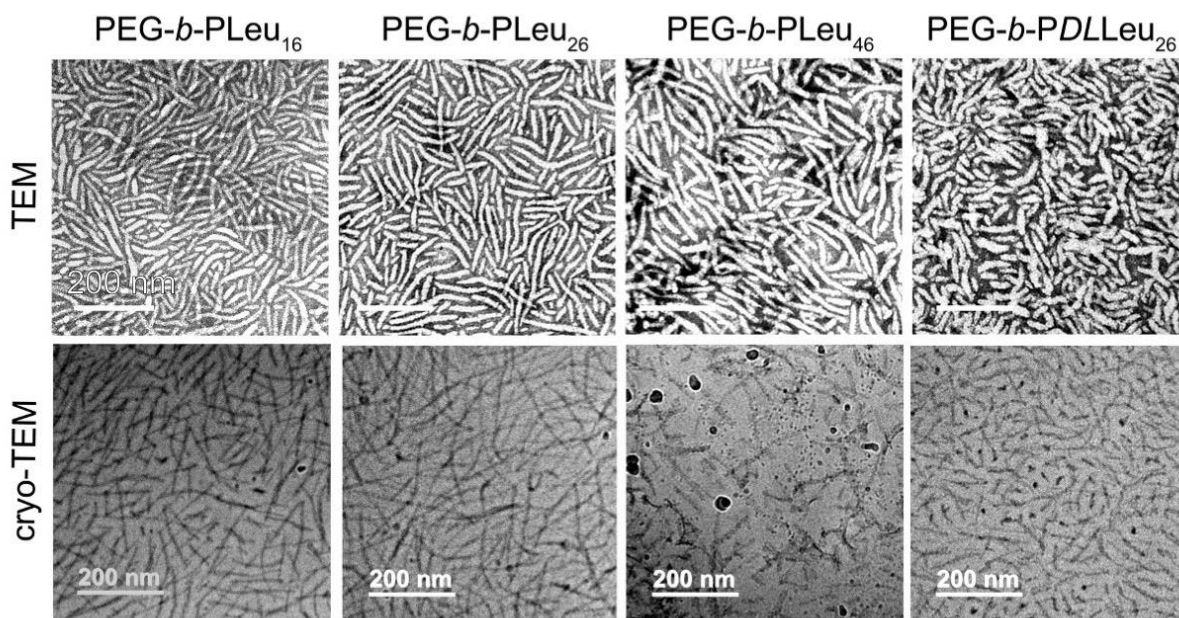


**Figure 3.** Electron microscopy images of copolymers **PEG-*b*-PLeu** obtained by ROPISA and dialyzed against ultra-pure water (top: TEM with negative staining using uranyl acetate, bottom: cryo-TEM).

To determine the effect of PLeu block size and chirality on PEG-*b*-PLeu morphology, we synthesized additional copolymers by varying the stoichiometry and the chirality of the Leu-NCA monomer with respect to the PEG<sub>5k</sub>-NH<sub>2</sub> macroinitiator (see table 1). Analysis of the copolymers by SEC in HFIP and <sup>1</sup>H NMR spectroscopy confirmed a low molar mass dispersity ( $\mathcal{D}$ ) around 1.20 and  $M_n$  values relatively consistent with the change in the  $[M]/[I]$  ratio (see table 1 and fig. S2, S7-S10). It should be noted that for **PEG-*b*-PLLeu<sub>46</sub>** and similar to **PEG-*b*-PBLG<sub>43</sub>**, the reaction medium becomes more and more viscous during the polymerization and results in the formation of soft gel. As before, we performed TEM and cryo-TEM of the new **PEG-*b*-PLLeu**

copolymers and compared the images to those obtained with **PEG-*b*-PLLeu<sub>26</sub>** (figure 3). TEM images of **PEG-*b*-PLLeu<sub>16</sub>**, having the shortest polypeptide block, showed rod-like nanomaterials, with narrow diameters (figure S14) and a slight trend of increase when the polypeptide block length increases to **PEG-*b*-PLLeu<sub>26</sub>** and then **PEG-*b*-PLLeu<sub>46</sub>**. On the other hand, copolymer **PEG-*b*-PDLLeu**, obtained from a racemic mixture of Leu-NCA, adopted less elongated but thicker nanostructures, underlining the importance of the amino acid NCA chirality with respect to the shape of the elongated morphologies formed in the process. Similar results were obtained using the racemic mixture BDLG NCA (**PEG-*b*-PBDLG**, see table 1 and figure S15). Overall, these observations from the dry samples were corroborated in solution using cryo-TEM imaging (figure 3) and by SAXS analysis (figure 4 and figure S13). In the intermediate  $q$ -range, a  $q^{-1}$  trend of the scattered intensity was consistent with the presence of rigid cylinders. Fitting the curves with the theoretical form factor model of polydisperse cylinders allowed estimation of the weight-average radius ( $R_w$ ) and length ( $L_w$ ) of the nanometric rods. From these determinations, much larger aspect ratios were found as compared to the **PEG-*b*-PBLG<sub>11-22</sub>** series (see table S1). Overall, and in agreement with the microscopy, the shape anisotropy of objects self-assembled by ROPISA with leucine monomer units appeared to be at least 3 – 5 times larger than with benzyl glutamate monomer units (figure S11).

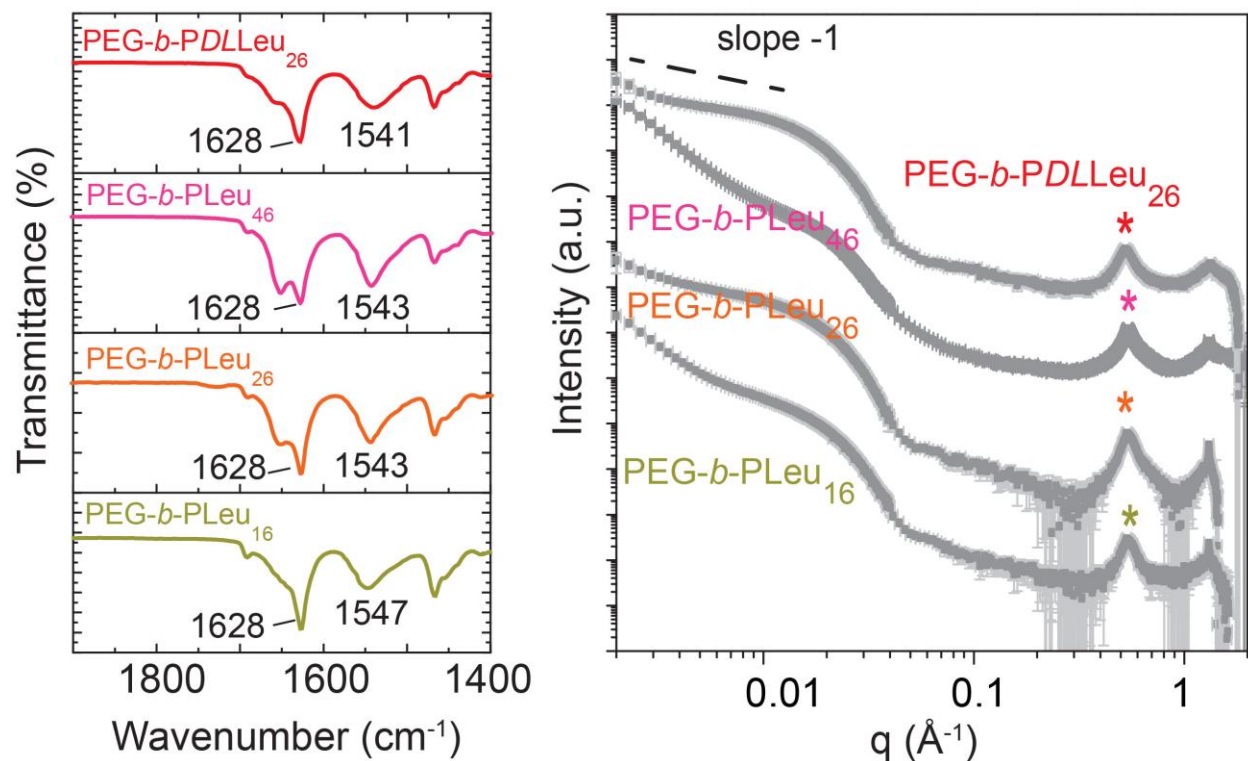


**Figure 4.** PEG-*b*-PLeu series of copolymers analyzed by FTIR on lyophilized powders (left) or by small-angle X-ray scattering (SAXS) as nanoparticles in ultra-pure water (right). For sake of clarity, two successive curves are offset by 2 decades in logarithmic scale ( $\times 10^2$ ).

Our results suggested that changing the NCA monomer to Leu-NCA increased the anisotropic character of the resulting self-assemblies. To better understand the origin of this larger anisotropy, we focused our attention on the secondary structure of the polypeptide block. In the high  $q$  range (WAXS), a clear Bragg diffraction peak at  $q^* = 0.533 \text{ \AA}^{-1}$  was observed for all copolymers containing poly(*L*-leucine), corresponding to a spacing of  $ca. 2\pi/q^* = 11.8 \text{ \AA}$ , very close to the spacing of  $11.9 \text{ \AA}$  reported for poly(leucine)<sup>49</sup> as ascribed to the repeating unit of laterally arrayed  $\beta$ -sheets. This observation clearly indicated that the packing of those secondary structures contributed to the elongated objects composed of the leucine-containing copolymers. It is worthwhile to note that racemic Leu-NCA also led to the formation of PLeu structured blocks

(figure 4), an indication that the ROPISA process could discriminate the polymerization of one enantiomer with respect to the other, a phenomenon of enantiomer separation generally found in crystallization processes. To corroborate the polypeptide conformation, we also collected FTIR spectra of the lyophilized dried powders of PEG-*b*-PLeu copolymers (figure 4). Copolymers PEG-*b*-PLeu clearly displayed a main amide I of  $\beta$ -sheet conformations ( $1628\text{ cm}^{-1}$ ), confirming all the packing observed in SAXS. In conclusion, and in marked contrast to samples containing PBLG blocks, our analyses showed that the PLeu polypeptide block mainly adopts  $\beta$ -sheet conformations, a crucial feature that significantly influenced the self-assembly behaviors observed in ROPISA.

#### 4. Conclusion

In summary, we report the combined one-pot synthesis and self-assembly of new amphiphilic copolymers from amino end-functionalized PEG macroinitiators using a single step aqueous ROPISA process of two different  $\alpha$ -amino acid N-carboxyanhydrides monomers, namely BLG-NCA and Leu-NCA. The ROPISA methodology yields concomitantly well-defined amphiphilic copolypeptide chains and self-assembled nanostructures in a rapid, facile, and straightforward process. The chemical nature of the NCA monomer and the secondary structure of the polypeptide define the dimensions parameters of the ROPISA afforded elongated nanostructures. In all cases, the nanostructures are rod-like self-assemblies and we have a good control over the diameter through the ROPISA preparation method. Nevertheless,  $\beta$ -sheet forming polypeptides such as PLeu strongly favor the formation of long rods with high aspect ratio, as compared to  $\alpha$ -helical polypeptides such as PBLG. Overall, this new ROPISA process enables efficient synthesis of rigid polypeptide-based nanomaterials at high solid contents with tunable anisotropy. Our results

demonstrate the versatility of the ROPISA method and open new avenues towards the design of functional nanomaterials.

## AUTHOR INFORMATION

### **Corresponding Author**

\*colin.bonduelle@enscbp.fr

\*lecommandoux@enscbp.fr

## ACKNOWLEDGMENT

The authors acknowledge Amelie Vax and Sylvain Bourasseau for assistance with size-exclusion chromatography and Jean Michel Guigner for assistance with cryo-TEM analyses. CG received support from a Marie-Curie fellowship from the European Union under the program H2020, Grant 749973 SENSOR. PSA received support from CONACYT (scholarship holder No. 548662). This work benefited from the use of the SasView application, originally developed under NSF Award DMR-0520547. SasView also contains code developed with funding from the EU Horizon 2020 program under the SINE2020 project Grant No 654000.

### ORCID numbers

Chloé Grazon 0000-0002-4564-8738

Pedro Salas 0000-0002-0922-4620

Segolene Antoine 0000-0002-4622-7062

Emmanuel Ibarboure 0000-0001-8614-3851

Elisabeth Garanger 0000-0001-9130-8286



Mark W. Grinstaff 0000-0002-5453-3668

Sébastien Lecommandoux 0000-0003-0465-8603

Colin Bonduelle 0000-0002-7213-7861

Olivier Sandre 0000-0002-1815-2702

Ben J. Boyd 0000-0001-5434-590X

Andrew J. Clulow 0000-0003-2037-853X

## REFERENCES

- (1) Whitesides, G. M.; Boncheva, M. *Proc. Natl. Acad. Sci.* **2002**, *99* (8), 4769–4774.
- (2) Shim, J.; Bates, F. S.; Lodge, T. P. *Nat. Commun.* **2019**, *10* (1), 1–7.
- (3) Lu, Y.; Lin, J.; Wang, L.; Zhang, L.; Cai, C. *Chem. Rev.* **2020**, *120* (9), 4111–4140.
- (4) Stupp, S. I.; Palmer, L. C. *Chem. Mater.* **2014**, *26* (1), 507–518.
- (5) Lehn, J. M. *Eur. Rev.* **2009**, *17* (2), 263–280.
- (6) Mai, Y.; Eisenberg, A. *Chem. Soc. Rev.* **2012**, *41* (18), 5969–5985.
- (7) Lee, M.; Cho, B. K.; Zin, W. C. *Chem. Rev.* **2001**, *101* (12), 3869–3892.
- (8) Tritschler, U.; Pearce, S.; Gwyther, J.; Whittell, G. R.; Manners, I. *Macromolecules* **2017**, *50* (9), 3439–3463.
- (9) Carlsen, A.; Lecommandoux, S. *Curr. Opin. Colloid Interface Sci.* **2009**, *14* (5), 329–339.
- (10) Cai, C.; Lin, J.; Lu, Y.; Zhang, Q.; Wang, L. *Chem. Soc. Rev.* **2016**, *45* (21), 5985–6012.

- (11) Bonduelle, C. *Polym. Chem.* **2018**, *9* (13), 1517–1529.
- (12) Rasines Mazo, A.; Allison-Logan, S.; Karimi, F.; Chan, N. J. A.; Qiu, W.; Duan, W.; O'Brien-Simpson, N. M.; Qiao, G. G. *Chem. Soc. Rev.* **2020**, *49* (14), 4737–4834.
- (13) Song, Z.; Han, Z.; Lv, S.; Chen, C.; Chen, L.; Yin, L.; Cheng, J. *Chem. Soc. Rev.* **2017**, *46* (21), 6570–6599.
- (14) Salas-Ambrosio, P.; Tronnet, A.; Verhaeghe, P.; Bonduelle, C. *Biomacromolecules* **2020**.
- (15) Bonduelle, C.; Lecommandoux, S. *Biomacromolecules* **2013**, *14* (9), 2973–2983.
- (16) Song, Z.; Fu, H.; Wang, R.; Pacheco, L. A.; Wang, X.; Lin, Y.; Cheng, J. *Chem. Soc. Rev.* **2018**, *47* (19), 7401–7425.
- (17) Shen, Y.; Fu, X.; Fu, W.; Li, Z. *Chem. Soc. Rev.* **2015**, *44* (3), 612–622.
- (18) Deming, T. J. *Chem. Rev.* **2016**, *116* (3), 786–808.
- (19) Song, Z.; Tan, Z.; Cheng, J. *Macromolecules* **2019**, *52* (22), 8521–8539.
- (20) D'Agosto, F.; Rieger, J.; Lansalot, M. *Angew. Chem, Int. Ed.* **2020**, *59* (22), 8368–8392.
- (21) Penfold, N. J. W.; Yeow, J.; Boyer, C.; Armes, S. P. *ACS Macro Lett.* **2019**, *8* (8), 1029–1054.
- (22) Derry, M. J.; Fielding, L. A.; Armes, S. P. *Prog. Polym. Sci.* **2016**, *52*, 1–18.
- (23) McLeary, J. B.; Klumperman, B. *Soft Matter* **2006**, *2* (1), 45–53.
- (24) Rieger, J. *Macromol. Rapid Commun.* **2015**, *36* (16), 1458–1471.

- (25) Yeow, J.; Boyer, C. *Adv. Sci.* **2017**, *4* (7).
- (26) Rieger, J.; Grazon, C.; Charleux, B.; Alaimo, D.; Jérôme, C. *J. Polym. Sci. Part A Polym. Chem.* **2009**, *47* (9), 2373–2390.
- (27) Tkachenko, V.; Matei Ghimbeu, C.; Vaultot, C.; Vidal, L.; Poly, J.; Chemtob, A. *Polym. Chem.* **2019**, *10* (18), 2316–2326.
- (28) Charleux, B.; Delaittre, G.; Rieger, J.; D’Agosto, F. *Macromolecules* **2012**, *45* (17), 6753–6765.
- (29) Warren, N. J.; Armes, S. P. *J. Am. Chem. Soc.* **2014**, *136* (29), 10174–10185.
- (30) Cao, C.; Chen, F.; Garvey, C. J.; Stenzel, M. H. *ACS Appl. Mater. Interfaces* **2020**, *12* (27), 30221–30233.
- (31) Blackman, L. D.; Varlas, S.; Arno, M. C.; Houston, Z. H.; Fletcher, N. L.; Thurecht, K. J.; Hasan, M.; Gibson, M. I.; O’Reilly, R. K. *ACS Cent. Sci.* **2018**, *4* (6), 718–723.
- (32) Jiang, J.; Zhang, X.; Fan, Z.; Du, J. *ACS Macro Lett.* **2019**, *8* (10), 1216–1221.
- (33) Grazon, C.; Salas-Ambrosio, P.; Ibarboure, E.; Buol, A.; Garanger, E.; Grinstaff, M. W.; Lecommandoux, S.; Bonduelle, C. *Angew. Chem, Int. Ed.* **2020**, *59* (2), 622–626.
- (34) Guégain, E.; Zhu, C.; Giovanardi, E.; Nicolas, J. *Macromolecules* **2019**, *52* (10), 3612–3624.
- (35) Hurst, P. J.; Rakowski, A. M.; Patterson, J. P. *Nat. Commun.* **2020**, *11* (1), 4690.
- (36) Salas-Ambrosio, P.; Tronnet, A.; Since, M.; Bourgeade-Delmas, S.; Stigliani, J.-L.; Vax,

- A.; Lecommandoux, S.; Dupuy, B.; Verhaeghe, P.; Bonduelle, C. *J. Am. Chem. Soc.* **2021**, *143* (10), 3697–3702.
- (37) Wright, D. B.; Touve, M. A.; Adamiak, L.; Gianneschi, N. C. *ACS Macro Lett.* **2017**, *6* (9), 925–929.
- (38) Kirby, N. M.; Mudie, S. T.; Hawley, A. M.; Cookson, D. J.; Mertens, H. D. T.; Cowieson, N.; Samardzic-Boban, V. *J. Appl. Crystallogr.* **2013**, *46* (6), 1670–1680.
- (39) Doucet, M.; Cho, J. H.; Alina, G.; Bakker, J.; Bouwman, W.; Butler, P.; Campbell, K.; Gonzales, M.; Heenan, R.; Jackson, A.; Juhas, P.; King, S.; Kienzle, P.; Krzywon, J.; Markvardsen, A.; Nielsen, T.; O'Driscoll, L.; Potrzebowski, W.; Ferraz Leal, R.; Richter, T.; Rozycko, P.; Snow, T.; Washington, A. *SasView Version 4.2*, Zenodo.; Zenodo, 2018.
- (40) Pedersen, J. S. *Adv. Colloid Interface Sci.* **1997**, *70*, 171–210.
- (41) Warren, N. J.; Derry, M. J.; Mykhaylyk, O. O.; Lovett, J. R.; Ratcliffe, L. P. D.; Ladmiral, V.; Blanazs, A.; Fielding, L. A.; Armes, S. P. *Macromolecules* **2018**, *51* (21), 8357–8371.
- (42) Brotherton, E. E.; Hatton, F. L.; Cockram, A. A.; Derry, M. J.; Czajka, A.; Cornel, E. J.; Topham, P. D.; Mykhaylyk, O. O.; Armes, S. P. *J. Am. Chem. Soc.* **2019**, *141* (34), 13664–13675.
- (43) Klok, H.-A.; Langenwalter, J. F.; Lecommandoux, S. *Macromolecules* **2000**, *33* (21), 7819–7826.
- (44) Lecommandoux, S.; Achard, M.-F.; Langenwalter, J. F.; Klok, H.-A. *Macromolecules* **2001**, *34* (26), 9100–9111.

- (45) McKinnon, A. J.; Tobolsky, A. V. *J. Phys. Chem.* **1968**, *72* (4), 1157–1161.
- (46) Klok, H. A.; Lecommandoux, S. *Adv. Mater.* **2001**, *13* (16), 1217–1229.
- (47) Manai, G.; Houimel, H.; Rigoulet, M.; Gillet, A.; Fazzini, P. F.; Ibarra, A.; Balor, S.; Roblin, P.; Esvan, J.; Coppel, Y.; Chaudret, B.; Bonduelle, C.; Tricard, S. *Nat. Commun.* **2020**, *11* (1), 1–7.
- (48) Nguyen, M.; Stigliani, J. L.; Bijani, C.; Verhaeghe, P.; Pratviel, G.; Bonduelle, C. *Biomacromolecules* **2018**, *19* (10), 4068–4074.
- (49) Fick, F.-G.; Semen, J.; Elias, H.-G. *Die Makromol. Chemie* **1978**, *179* (3), 579–590.